Proposed Panel Zone Model for Seismic Design of Steel Moment-Resisting Frames

Andronikos Skiadopoulos, S.M.ASCE[1]; Ahmed Elkady, Ph.D.[2]; Dimitrios G. Lignos, M.ASCE[3*]

Abstract: This paper proposes a new mechanics-based model for the seismic design of beam-to-column panel zone joints in steel moment-resisting frames. The model is based on realistic shear stress distributions retrieved from continuum finite element (CFE) analyses of representative panel zone geometries. Comparisons with a comprehensive experimental dataset suggest that the proposed model predicts the panel zone stiffness and shear strength with a noteworthy accuracy even in panel zones featuring columns with thick flanges (thicker than 40mm), as well as in cases with high beam-to-column aspect ratios (larger than 1.5). In that respect, the proposed model addresses the limitations of all other available models in the literature. If doubler plates are deemed necessary in the panel zone design, the CFE simulations do not depict any doubler-to-column web shear stress incompatibility, provided that the current detailing practice is respected. Hence, the total thickness of the column web and doubler plates should be directly used in the proposed panel zone model. The panel zone shear strength reduction due to the axial load effects should be based on the peak axial compressive load including the transient component due to dynamic overturning effects in exterior joints. It is found that the commonly used von Mises criterion suffice to adequately predict the shear strength reduction in the panel zone.

Keywords: steel moment resisting frames; panel zone shear resistance; beam-to-column connections; panel zone model; balanced design; doubler plate ineffectiveness;

[1] Doctoral Assistant, RESSLab, ENAC, École Polytechnique Fédérale de Lausanne (EPFL), Station 18, Lausanne 1015, Switzerland. E-mail: andronikos.skiadopoulos@epfl.ch

[2] Lecturer, University of Southampton, Southampton, SO16 7QF, United Kingdom. E-mail: a.elkady@soton.ac.uk [formerly, post-doctoral research scientist, RESSLab, ENAC, École Polytechnique Fédérale de Lausanne (EPFL)]

[3] Associate Professor, RESSLab, ENAC, École Polytechnique Fédérale de Lausanne (EPFL), Station 18, Lausanne 1015, Switzerland (*corresponding author). E-mail: dimitrios.lignos@epfl.ch

Introduction

In capacity-designed steel moment resisting frame (MRF) systems, a balanced beam-to-column connection design is promoted. In principle, the panel zone joint may experience limited inelastic behavior. A challenge to mobilize the panel zone in the seismic energy dissipation, is the increased potential of premature connection fracture, when improperly detailed (Chi et al. 1997; El-Tawil et al. 1999; Lu et al. 2000; Mao et al. 2001; Ricles et al. 2000, 2004).

Experimental research (Kim and Lee 2017; Lee et al. 2005; Shin and Engelhardt 2013) indicates that a properly detailed fully restrained beam-to-column joint designed with controlled panel zone yielding may lead to an improved seismic performance compared to what is perceived as a "strong" panel zone design (where the panel zone remains elastic). In particular, data from assembled inelastic panel zone databases (http://resslabtools.epfl.ch; El Jisr et al. 2019; Skiadopoulos and Lignos 2020) suggest that at story drift demands corresponding to 4% rad, modern fully-restrained beam-to-column connections (AISC 2016a) do not experience premature weld fractures when their panel zone joints attain shear distortions up to $10\gamma_y$, (where γ_y is the panel zone yield shear distortion angle). Others (Chi and Uang 2002; Ricles et al. 2004) found that when panel zones exhibit inelastic behavior within a steel MRF beam-to-column connection, the column twist demands due to beam plastic hinge formation become fairly minimal. This issue is prevalent in steel MRF designs featuring deep columns, which are prone to twisting (Elkady and Lignos 2018a; b; Ozkula et al. 2017). To reliably mobilize the inelastic behavior of a panel zone, its shear stiffness and strength should be accurately predicted during the steel MRF seismic design phase.

Models to simulate the inelastic panel zone behavior in terms of shear strength, V_{pz}, and shear distortion angle, γ, are available in the literature (Fielding and Huang 1971; Kato et al. 1988; Kim and Engelhardt 2002; Krawinkler 1978; Lee et al. 2005; Wang 1988). Referring to Fig. 1 and Eq. (1), these models comprise a shear-dominated elastic stiffness, K_e, up to the yield shear strength, V_y [see Eq. (2)]. This is deduced by assuming a uniform shear stress distribution in the column web. An inelastic hardening branch with post-yield stiffness, K_p, defines the panel zone's post-yield behavior up to a shear strength, V_p [see Eq. (3)], at $4\gamma_y$. This strength accounts for the contribution of the surrounding elements (continuity plates and column flanges). Finally, a third branch, where the shear strength is assumed to stabilize, is typically accounted for with a post-γ_p slope that is expressed as percentage of the elastic stiffness, as discussed later on.

$$K_e = \frac{V_y}{\gamma_y} = 0.95 \cdot d_c \cdot t_{pz} \cdot G \tag{1}$$

$$V_y = \frac{f_y}{\sqrt{3}} \cdot 0.95 d_c \cdot t_{pz} \tag{2}$$

$$V_p = \mathrm{V_y} \cdot \left(1 + 3K_p/K_e\right) \tag{3}$$

Where the panel zone thickness, $t_{pz} = t_{cw} + t_{dp}$ in case doubler plate(s) are present; t_{cw} is the thickness of the column web; t_{dp} is the total thickness of the doubler plates(s); d_c is the column depth; f_y is the steel material yield stress; G is the steel material modulus of rigidity. The bending deformation of the panel zone (see Fig. 1b) is neglected in this case.

Krawinkler (1978) proposed the trilinear model (hereinafter referred as Krawinkler model) shown in Fig. 1c, which has been adopted in current design provisions with minor modifications throughout the years (AISC 2016b; CEN 2005). Once the panel zone yields uniformly at γ_y, the Krawinkler model assumes that the column web is not capable of withstanding any additional shear. Depending on the column cross-section profile, its flanges and continuity plates (if installed) participate in resisting the post-yield panel zone shear demand. Referring to Fig. 1c, the post-yield stiffness, K_p, of the Krawinkler model was derived using the principle of virtual work for the panel zone kinking locations based on small-scale subassembly experiments (flange thickness between 10 and 24mm). Referring to Fig. 1c, the above model is valid up to $\gamma_p = 4\gamma_y$. Alternative γ_p values are proposed in literature by other researchers. For instance, Wang (1988) proposed a value of $3.5\gamma_y$ whereas Kim et al. (2015) related this value mathematically with the joint's geometric and material properties. The post-γ_p stiffness is usually taken as 3% of K_e (Gupta and Krawinkler 2000; PEER/ATC 2010; Slutter 1981) acknowledging that the shear resistance is only attributed to material strain hardening. Krawinkler (1978) suggested that for joints comprising stocky columns (flanges thicker than 30 to 40mm), further experiments should be conducted to verify the predicted shear strength of his model.

Considering the assumptions and limitations of this model (Brandonisio et al. 2012; El-Tawil et al. 1999; Jin and El-Tawil 2005; Kim and Engelhardt 2002; Krawinkler 1978; Lee et al. 2005; Qi et al. 2018; Soliman et al. 2018), several researchers attempted to propose more robust $V_{pz} - \gamma$

relations. In some of these studies (Castro et al. 2005; Chung et al. 2010; Han et al. 2007; Kim et al. 2015; Lee et al. 2005), the resultant V_y was more-or-less similar to that of the Krawinkler model [i.e., Eq. (2)] excluding distinct differences in the assumed effective shear area. The post-yield stiffness, K_p, was refined empirically based on available experimental data. Tsai and Popov (1988) showed that the average shear stress in the panel zone is 20% lower than the peak shear stress developed in the panel zone web center; thereby suggesting that the uniform shear distribution for calculating V_y is impracticable (Charney et al. 2005; Chung et al. 2010; Kim and Engelhardt 2002; Lin et al. 2000). Kim and Engelhardt (2002) and Lin et al. (2000) formulated the above findings in an empirical fashion based on limited experimental data featuring column flange thicknesses less than 35mm. Other studies leveraged the finite element method to examine the panel zone inelastic behavior (Hjelmstad and Haikal 2006; Krishnan and Hall 2006; Léger et al. 1991; Li and Goto 1998; Mulas 2004) without reaching to a consensus for an improved panel zone model to be used in the seismic design of steel MRFs.

From a design standpoint, panel zone joints may moderately participate in energy dissipation during an earthquake according to the North American provisions (AISC 2016c; CSA 2019). The code-based design shear strength (either the panel zone shear yield strength, $R_{n,el.}$, or post-yield strength, $R_{n,pl.}$) is computed based on the Krawinkler model (i.e., V_y and V_p, respectively). In Japan (AIJ 2012), the panel zone shear strength is computed as per $R_{n,el.}$ AISC (2016b), with the difference that $1/\sqrt{3}$ is considered instead of the 0.6 factor. However, the panel zone shear demand imposed from beams is reduced by 25% to implicitly contemplate the neglected column shear force contribution and the disregarded panel zone post-yield strength. In Europe, CEN (2005) considers the contribution of the column web in a similar manner with $R_{n,el.}$. If continuity plates are present, an additional term is enumerated to compute the panel zone shear strength. This term is based on the plastic moment resistance of the column flanges at the kinking locations (see Fig. 1a).

Figure 2 depicts the analytically-derived elastic stiffness, K_e, of various panel zone geometries with/without doubler plates versus the measured one, $K_{e,m}$, from collected full-scale experiments (Skiadopoulos and Lignos 2020). In the case of test data without doubler plates, Fig. 2a suggests that common panel zone models (CEN 2005; Kim and Engelhardt 2002; Krawinkler 1978) overestimate K_e by up to 30%. This is attributed to the uniform yielding assumption at γ_y along with the depreciation of the panel zone bending deformation mode (see Fig. 1b) depending on the panel zone aspect ratio and column flange thickness.

Compelling issues with conflicting observations are also found in cases where doubler plates are utilized to reach a desirable panel zone shear strength. Depending on the weld details, the doubler plate efficiency (ratio of shear stresses in the doubler plate to those in the column web) does not exceed 50% (Kim and Engelhardt 2002); hence half of their thickness, at most, is participating in the connection stiffness and strength. For this reason, CEN (2005) accounts only for one doubler plate even when two plates are required by design. Referring to Fig. 2b, the data suggests that K_e , based on CEN (2005), is underpredicted by nearly 20%. Lee et al. (2005) found that fillet welded doubler plates to the column web, according to the AISC (2016c) provisions, allow for excellent stress compatibility between the plates and the column web. These conclusions are in line with earlier work on fillet-welded doubler plates (Bertero et al. 1973) and on complete joint penetration (CJP) welded plates (Ghobarah et al. 1992). More recently, Shirsat and Engelhardt (2012) showed that the stress compatibility between the column web and the doubler plate is lower for deep columns utilizing thick doubler plates (plate thicknesses, $t_{dp} \geq 26$mm). Referring to Fig. 2b, the AISC panel zone model that accounts for both doubler plates (if applicable) generally overestimates K_e.

Figure 3a depicts the deviation of the analytically-predicted post-yield stiffness, K_p (as per AISC 2016b and Lee et al. 2005), from the measured one, $K_{p,m}$ with respect to the column flange thickness, t_{cf}. For t_{cf} larger than 40mm, K_p, at a targeted shear distortion angle of $4\gamma_y$, is over-predicted by up to 40% as per the AISC (2016b) model. Referring to Fig. 3b, same observations hold true for V_p according to the AISC (2016b) panel zone model. Note that for the cyclic test data, the extraction of the panel zone measured parameters of interest is based on the average values of the positive and negative first cycle envelopes as shown in Fig. 3c. The panel zone measured strength at γ_y and $4\gamma_y$ is, then, determined and, as such, $K_{p,m}$ is defined based on these two reference points. The model by Lee et al. (2005) consistently underestimates K_p (see Fig. 3a) since it was benchmarked with limited data from assemblies comprising columns with flange thicknesses less than 30mm. The Kim et al. (2015) model assumes that the post-yield panel zone response is controlled by the plastic column flange bending capacity under normal stresses. However, this assumption, which is the same with the CEN (2005) panel zone model, is unconservative for steel columns featuring thick flanges (i.e., $t_{cf} > 50$mm) (see Fig. 3b). These attract a considerable amount (up to 40%) of the total shear force.

To capture the interaction of axial load and shear within the panel zone joint, a reduction factor $r = \sqrt{1 - n^2}$, (where, $n = P/P_y$, P and P_y are the applied axial compressive load and axial yield strength of a steel column, respectively) has been proposed (Chung et al. 2006; Krawinkler 1978). This is based on the von Mises criterion (von Mises 1913). This is also consistent with the Japanese provisions (AIJ 2012). In the US, a panel zone shear strength reduction is employed according to a fit to the $r - n$ curve, when the panel zone is designed based on $R_{n,el.}$ (AISC 2016b). Otherwise, a reduction factor is applied to improbably high axial load demands ($n > 0.75$). This tends to overestimate the panel zone shear strength by nearly 15% for $n = 0.5$. In Europe, regardless of the axial demand-to-capacity ratio of the column, the shear resistance is accounted for through a constant reduction factor of 0.9 (Ciutina and Dubina 2003).

To address the above challenges, this paper proposes a mechanics-based panel zone model that could be potentially used for the seismic design of steel MRF systems. This model is informed by continuum finite element (CFE) analyses validated to available experimental data. Panel zone joints are categorized according to the shear stress evolution in the column web and flanges. Moreover, improved panel zone shear strength equations that account for the realistic stress distributions within the web panel and column flanges at three levels of shear distortions (γ_y, $4\gamma_y$ and $6\gamma_y$) are proposed. The doubler plate stress compatibility with the column web is also examined for panel zone configurations comprising CJP and fillet weld details according to today's construction practice. The axial load effect on the panel zone shear strength and stiffness is also examined for both interior and end columns within steel MRFs in an effort to generalize the proposed model.

Mechanics of panel zone behavior through continuum finite element analysis

A CFE model is developed to examine the stress profile within a panel zone joint at various levels of inelastic shear distortion. The commercial finite element analysis software ABAQUS (version 6.14-1) (ABAQUS 2014) is used for this purpose. This section describes the CFE modeling approach and its validation along with the main panel zone parameters of interest. The CFE model validation is demonstrated with two full-scale beam-to-column connection tests. The first test [specimen UCB-PN3, FEMA (1997)] features an exterior subassembly with a stocky column (W14x257) and a 900mm deep beam (W36x150). The second test [specimen SPEC-6, Ricles et al. (2004)] features an interior subassembly with deep members (W30x108 beams and a W24x131 column). All members were fabricated from Gr. 50 steel (nominal yield stress, $f_y = 345$MPa).

Description and validation of the CFE modeling approach

The CFE model, which is shown in Fig. 4a, constitutes twenty-node quadratic brick elements (C3D20R) with reduced integration and a maximum dimension of 20mm. These elements do not typically experience hourglassing and/or shear locking effects. To determine the optimum element type and mesh size, a mesh sensitivity analysis is conducted with four element types (i.e., C3D20, C3D20R, C3D8, C3D8R). Moreover, local imperfections in the beams are incorporated according to the first critical buckling eigenmode. Web imperfections are deemed critical and are tuned to an amplitude of $d_b/250$, which is consistent with prior related studies (Elkady and Lignos 2018b). Residual stresses according to Young (1972) are incorporated in the deep members. For the W14x257 column, the residual stress distribution by de Castro e Sousa and Lignos (2017) is adopted. The CFE model captures the steel material nonlinearity with a multiaxial combined isotropic/kinematic hardening law (Lemaitre and Chaboche 1990) within the J2 plasticity constitutive model (von Mises 1913). The input model parameters are based on prior work by de Castro e Sousa et al. (2020). Referring to Fig. 4b, the CJP welds along the perimeter of the doubler plate are explicitly modeled. Four plug welds are simulated with 15mm fasteners that constrain all six degrees-of-freedom. The continuity plates are tied in the column flanges and the doubler plate. Referring to Fig. 5, the agreement between the measured and simulated results both at the global (load-story drift ratio response) and local level (panel zone shear force-shear distortion response) is noteworthy regardless of the inelastic shear distortion. As for the UCB-PN3 specimen, the agreement of the simulated and measured data with regard to the global behavior is noteworthy (see Fig. 5a). In Fig. 5b, the simulated panel zone response agrees well with the test data up to an inelastic shear distortion of 0.5% rad (i.e., semi-last loading cycle). After reviewing the experimental report (Popov et al. 1996), it is found that the reason for the observed discrepancy between the measured and simulated panel zone response is the occurrence of beam weld fracture in the semi-last loading cycle. This was not simulated in the CFE model. After the occurrence of weld fracture, the shear demand in the panel zone reduced, thereby decreasing the associated inelastic shear distortion. This is also confirmed from UCB-PN1 specimen, from the same test program, that involved a nominally identical subassembly with UCB-PN3. However, premature fracture occurred at a much later loading cycle.

In an effort to expedite the computations, a reduced-order panel zone CFE model is also developed as shown in Fig. 4c. This model does not include the continuity plates. Instead, a "Rigid Body" constraint is applied at the column's top and bottom edges (i.e., at the locations of the beam flanges) to prevent stress concentrations during the imposed loading. According to the AISC (2016b) specifications, continuity plates are deemed necessary when the column cannot withstand the beam flange concentrated forces. Unlike slender column profiles, in stocky ones, the column itself is able to sustain the concentrated beam forces, hence continuity plates may be disregarded (see Section E3.6f, AISC 2016c). Besides, the panel zone strength and stiffness parameters would not be influenced by the presence of continuity plates. Accordingly, assuming fixed end boundaries is justifiable for both cases. Out-of-plane displacements and rotations as well as in plane rotations are restrained at the panel zone edges. Hence the panel zone joint behaves as a beam in contra-flexure. Referring to Figs. 5b and 5d, the simulated responses based on the detailed and reduced-order models are nearly identical for the examined subassemblies. Therefore, the reduced-order panel zone CFE model is adopted hereinafter.

Deduced Panel Zone Performance Parameters

The simulation matrix comprises eight panel zone geometries. These are designed to have the same V_y with specimen UCB-PN3, i.e., the column web thickness and depth are kept constant. The varied geometric parameters are the panel zone aspect ratio, d_b/d_c, the column flange width, b_{cf}, and the column flange thickness, t_{cf}. The first two parameters are chosen to examine the effect of the bending deformation mode on K_e, whereas t_{cf} is chosen to examine the influence of the column flange thickness on the panel zone shear strength. The panel zone models are subjected to monotonic inelastic shear distortions up to $6\gamma_y$.

Figure 6 shows the primary panel zone performance parameters of interest. The elastic panel zone shear stiffness, K_e, is deduced from the elastic branch slope of the $V_{pz} - \gamma$ behavior. The yield strength, V_y, is deduced based on the yield initiation according to the von Mises criterion (von

Mises 1913) in the panel zone center. Finally, the post-yield panel zone shear strength is deduced at two representative shear distortion levels, $4\gamma_y$ (V_p) and $6\gamma_y$ ($V_{6\gamma_y}$). The latter is considered, since there may be appreciable reserve shear strength attributed to the column flange contribution along with strain hardening due to column web shear yielding.

Discussion

Figure 7 shows a comparison between representative CFE simulations for various panel zone aspect ratios, d_b/d_c and the predicted behavior according to the Krawinkler model. As expected, the figure suggests that the deviation of the predicted elastic stiffness, K_e [Eq. (1)], the yield strength, V_y [Eq. (2)] and post-yield strength, V_p [Eq. (3)] from the CFE results may be appreciable depending on the panel zone aspect ratio and the column flange thickness. Particularly, for slender panel zones (i.e., d_b/d_c=1.5 and t_{cf} =24mm) the measured elastic stiffness is about 30% lower than the predicted one since the Krawinkler model neglects the bending contribution (see Fig. 1b). However, for stocky and shallow panel zones with an aspect ratio of one and thick flanges ($t_{cf} \cong$ 50mm), where the shear deformation mode is dominant, the Krawinkler model predicts K_e reasonably well. Though, the panel zone stiffness is still underpredicted by 10-15% due to the assumed effective shear area (Charney et al. 2005). Same observations hold true for V_y. The Krawinkler model overestimates V_p by more than 20% for stocky and shallow panel zones. For the cross-section range that the same model was calibrated for, the post-yield shear strength is only overestimated by up to 10%.

The above deviations can be justified by examining the stress distributions within the panel zone. Figure 8 shows the shear stress distributions for two characteristic panel zone geometries, normalized by the yield shear stress, τ_y ($\tau_y = f_y/\sqrt{3}$), at a shear distortion angle equal to γ_y, $4\gamma_y$ and $6\gamma_y$. The shear stress distributions are extracted from the column cross-section corresponding to the beam centerline. Superimposed in the same figure are planes representing the average shear stress in the column web. Referring to Fig. 8a, the common assumption of a uniform shear distribution in the column web is not rational for slender panel zones, particularly at shear distortions near yielding, whereas the column flange contribution to shear yielding is indeed negligible.

Referring to Fig. 8b, stocky and shallow panel zones experience almost uniform shear stresses in their web regardless of the shear angle distortion. The contribution of the column flanges to the attained shear stresses (maximum of $4\%\tau_y$) may seem insignificant for shear distortion levels of γ_y. However, since the flange area of stocky cross-sections outweighs that of their web, the resultant force is appreciable (15-40% of the total panel zone shear force, depending on the shear distortion level).

Proposed panel zone model

Panel zone elastic stiffness

The proposed panel zone elastic stiffness, K_e [see Eq. (4)], is derived based on both shear and bending deformation modes as shown in Fig. 1. The shear mode is accounted for based on Eq. (5). The bending mode is deduced based on the elastic stiffness (in terms of $V_{pz} - \gamma$ relation) of a beam in contra-flexure according to Eq. (6).

$$K_e = \frac{V_{pz}}{\gamma} = \frac{K_s \cdot K_b}{K_s + K_b} \tag{4}$$

$$K_s = A_v \cdot G = t_{pz} \cdot (d_c - t_{cf}) \cdot G \tag{5}$$

$$K_b = \frac{12 \cdot E \cdot I}{d_b^3} \cdot d_b \tag{6}$$

The proposed model assumes a panel zone shear strength equilibrium instead of shear deformation compatibility. Therefore, the proposed panel zone stiffness is computed based on Eq. (4) by considering the two deformation modes in series (i.e., $\gamma = \gamma_{shear} + \gamma_{bending}$) (see Fig. 1). In Eqs. (4) to (6), I is the second moment of area of the panel zone cross section (including the doubler plate(s) thickness, if any) with respect to the column's strong-axis; and A_v is the effective shear area according to Charney et al. (2005). Although other panel zone models (AISC 2016b; Fielding and Huang 1971; Kato et al. 1988; Lui and Chen 1986; Mulas 2004) assume an effective depth, $d_{eff} = d_c$, the panel zone shear stiffness (and strength) tends to be overestimated by about 10% for stocky column cross-sections (t_{cf} > 40mm) based on the above assumption. Note here that the second moment of area, I, refers to that of the full column cross-section. Other researchers that attempted to address the bending deformation mode issue (Kim et al. 2015), accounted for the column flange deformation mode independently from the column web.

Panel zone shear strength

To predict a realistic yield and post-yield panel zone shear strength, the shear stress distributions in the panel zone from Fig. 8 are employed. The panel zone shear force, V_{pz}, at a distortion, γ, may be approximated by Eq. (7) where, V_f is the shear force resisted by a single column flange; V_w is the shear force resisted by the column web. In turn, V_f may be assumed to be proportional to the ratio of the column flange stiffness, K_f, to the panel zone's elastic stiffness, K_e, according to Eq. (8). The column flange stiffness may be computed using Eq. (9) by considering both shear and bending deformation modes as depicted by Eqs. (10) and (11), respectively.

$$V_{pz} = 2V_f + V_w \tag{7}$$

$$V_f = (K_f/K_e) \cdot V_{pz} \tag{8}$$

Equation (10) assumes a uniform shear stress distribution in the column flanges, while Eq. (11) assumes contra-flexure deformation with respect to the weak-axis of the column flanges.

$$K_f = \frac{K_{sf} \cdot K_{bf}}{K_{sf} + K_{bf}} \tag{9}$$

$$K_{sf} = 2 \cdot (t_{cf} \cdot b_{cf} \cdot G) \tag{10}$$

$$K_{bf} = 2 \cdot \left[\frac{12E(b_{cf} \cdot t_{cf}^3/12)}{d_b^3} \cdot d_b\right] \tag{11}$$

In the above equations, the K_f/K_e ratio provides an estimate of the panel zone shear force resisted by the column flanges. Particularly, Fig. 9a shows how K_f/K_e influences the deduced K_e for the examined panel zone geometries discussed earlier. In the vertical axis, these parameters are either predicted by the proposed or the Krawinkler model. The predicted stiffness, K_e, is normalized by the deduced, $K_{e,m}$ from the CFE results. The dashed line at an abscissa value of 1.0 represents the ideal agreement between the virtual tests and the analytical model predictions.

Referring to Fig. 9a, the proposed panel zone stiffness from Eq. (4) shows improved accuracy over the Krawinkler model particularly for slender panel zone geometries ($K_f/K_e < 0.02$). For stocky and shallow panel zone geometries ($K_f/K_e > 0.07$), the effective area limitation as per Charney et al. (2005) leads to at least the same accuracy as the Krawinkler model since the bending deformation mode is negligible.

Figure 9b shows the normalized post-yield panel zone stiffness, K_{γ_i}, at various shear distortions (i.e., $4\gamma_y$, $5\gamma_y$ and $6\gamma_y$), with respect to K_f/K_e. The K_{γ_i} is deduced from the tangential slope of the $V_{pz}-\gamma$ relation. Note that beyond $4\gamma_y$, the tangent stiffness is used to provide a consistent comparison with the constant $0.03K_e$ post-$4\gamma_y$ that has been historically assumed in literature (Gupta and Krawinkler 2000; Slutter 1981). This figure suggests that at $4\gamma_y$, the post-yield panel zone stiffness reaches $0.07K_e$, whereas at $6\gamma_y$ attains $0.04K_e$. The K_{γ_i}/K_e, at $4\gamma_y$, of stocky and shallow panel zones ($K_f/K_e > 0.07$) becomes double compared to slender ones. Consequently, the empirical post-$4\gamma_y$ stiffness of $0.03K_e$ (Gupta and Krawinkler 2000; PEER/ATC 2010; Slutter 1981) is irrational for most panel zone geometries. Instead, the panel zone shear strength at a shear distortion angle of $6\gamma_y$ should be used with V_p to define the respective slope. This may also be more effective for optimal balanced design of beam-to-column joints in capacity-designed steel MRFs. Large panel zone shear distortions may raise concerns regarding localised deformations, consequential implications on system level response and increased potential for weld fractures (Chi et al. 1997; El-Tawil et al. 1999; Lu et al. 2000; Mao et al. 2001; Ricles et al. 2000, 2004). However, experimental data from recently compiled databases with over 100 post-Northridge bare steel and composite-steel beam-to-column connections (El-Jisr et al. 2019; Skiadopoulos and Lignos 2020) that exhibited inelastic behavior in their web panels, did not experience premature fracture even at inelastic shear distortions up to $10\gamma_y$ as discusser earlier.

The panel zone shear strength can be generally computed using Eq. (12) by summing up the surface integral of the shear stresses along the panel zone's web and flange areas. A realistic shear stress distribution should be deduced at a given shear distortion level for this purpose. Given the discrete finite element mesh, the surface integral in Eq. (12) can be replaced by the double summation of the shear stresses as given by Eq. (13).

$$V_{pz} = \int_A \tau dA = \int_{A_w} \tau dA_w + 2\int_{A_f} \tau dA_f \tag{12}$$

The parameters a_w and a_f, introduced in Eq. (13), represent the shear stress of each element in the column web and each flange, respectively, normalized by the shear stress at yielding, τ_y. In these equations, the yield stress of the web and flanges is assumed to be the same. Since the column flanges and web element size was kept constant in the CFE model, Eq. (13) can be re-written as in Eq. (14).

$$V_{pz} = \frac{f_y}{\sqrt{3}} \cdot \sum_{-d_c/2}^{d_c/2} \sum_{-t_{cw}/2}^{t_{cw}/2} a_w(x,y)\delta_x\delta_y + \frac{f_y}{\sqrt{3}} \cdot 2 \sum_{-b_{cf}/2}^{b_{cf}/2} \sum_{-t_{cf}/2}^{t_{cf}/2} a_f(x,y)\delta_x\delta_y \tag{13}$$

$$V_{pz} = \frac{f_y}{\sqrt{3}} \cdot \frac{d_c \cdot t_{cw}}{N_w} \cdot \sum_{-d_c/2}^{d_c/2} \sum_{-t_{cw}/2}^{t_{cw}/2} a_w(x,y) + \frac{f_y}{\sqrt{3}} \cdot 2 \frac{(b_{cf} - t_{cw}) \cdot t_{cf}}{N_f} \cdot \sum_{-b_{cf}/2}^{b_{cf}/2} \sum_{-t_{cf}/2}^{t_{cf}/2} a_f(x,y) \tag{14}$$

Where, N_w and N_f are the number of finite elements of the web and each flange, respectively. Finally, as per Eq. (15), the panel zone shear strength can be expressed in terms of a_{eff} [see Eq. (16)], which is the average shear stress within the column flanges or web (i.e., sum of all stresses divided by number of elements in a given component), normalized by τ_y.

$$V_{pz} = a_{w,eff} \cdot \frac{f_y}{\sqrt{3}} \cdot (d_c - t_{cf}) \cdot t_{cw} + a_{f,eff} \cdot \frac{f_y}{\sqrt{3}} \cdot (b_{cf} - t_{cw}) \cdot 2t_{cf} \tag{15}$$

$$a_{w,eff} = \frac{\sum_{-d_c/2}^{d_c/2} \sum_{-t_{cw}/2}^{t_{cw}/2} \tau_w \delta x \delta y}{t_{cw} \cdot (d_c - t_{cf}) \cdot \tau_y}, \text{ and } a_{f,eff} = \frac{\sum_{-b_{cf}/2}^{b_{cf}/2} \sum_{-t_{cf}/2}^{t_{cf}/2} \tau_f \delta x \delta y}{t_{cf} \cdot b_{cf} \cdot \tau_y} \tag{16}$$

Figure 10 illustrates the normalized average shear stresses of the column web and flanges from Eq. (16), as a function of K_f/K_e, at shear distortions of γ_y, $4\gamma_y$ and $6\gamma_y$. The linear regression curves for these relationships are superimposed in this figure and their statistical values (mean, standard deviation and coefficient of determination, R^2) are summarized in Table 1 for reference. Figure 10a suggests that in general, and even for high shear distortions ($\gamma = 6\gamma_y$), the influence of K_f/K_e on the column web stress contribution is not significant as inferred by the mild slope of the fitted trend lines. Quantitatively, this is expressed by the miniscule standard deviation values shown in Table 1 at $4\gamma_y$ and $6\gamma_y$. Accordingly, the average stress of the web at these distortions may be approximated by a single value regardless of the panel zone geometry. Referring to Fig. 10b, when $K_f/K_e > 0.07$ (stocky panel zones), the average stress of the column flange is appreciable for shear distortions larger than γ_y. In contrast, for slender panel zones ($K_f/K_e < 0.02$), the column flange average stress is negligible; hence, the column flange contribution to the panel zone shear strength is not important.

A set of panel zone shear strength equations at γ_y (i.e., V_y), $4\gamma_y$ (i.e., V_p) and $6\gamma_y$ (noted as $V_{6\gamma_y}$) are proposed in support of contemporary seismic design of steel MRFs. According to Eq. (17), the proposed, V_y, is as follows,

$$V_y = \frac{[0.58(K_f/K_e) + 0.88] \cdot \frac{f_y}{\sqrt{3}} \cdot (d_c - t_{cf}) \cdot t_{cw}}{1 - K_f/K_e} = \frac{f_y}{\sqrt{3}} \cdot a_y \cdot (d_c - t_{cf}) \cdot t_{cw} \quad (17)$$

where $a_y = 0.9$ and 1.0 for slender and stocky panel zones, respectively. Note that for stocky panel zones, Eq. (17) matches that of the Krawinkler model.

The proposed panel zone shear strength for V_p and $V_{6\gamma_y}$ is given by Eq. (18) along with recommended values for $a_{w,eff}$ and $a_{f,eff}$ in Table 2 directly extracted from representative shear stress profiles of panel zone geometries. Interpolation may be used for the corresponding a_{eff} values when the panel zone geometry is neither slender nor stocky (i.e., $K_f/K_e = 0.02$ to 0.07).

$$V_{pz} = \frac{f_y}{\sqrt{3}} \cdot [a_{w,eff} \cdot (d_c - t_{cf}) \cdot t_{cw} + a_{f,eff} \cdot (b_{cf} - t_{cw}) \cdot 2t_{cf}] \quad (18)$$

Proposed panel zone model validation

Figure 11 shows a comparison of the panel zone's hysteretic response from characteristic full-scale tests (Ricles et al. 2004; Shin 2017) and the predicted envelope curve based on the proposed model. For reference, the AISC (2016b) model is superimposed in the same figure. The additional third branch slope of $0.03K_e$ is also considered beyond V_p (Gupta and Krawinkler 2000; PEER/ATC 2010; Slutter 1981). The comparisons highlight the superior accuracy of the proposed model in predicting the panel zone's shear strength and stiffness over the AISC model, which consistently overestimates the same quantities by nearly 30%. Moreover, the assumed $0.03K_e$ stiffness in the third branch is not justifiable for slender panel zones as discussed earlier (see Fig. 11a).

An assembled inelastic panel zone database (Skiadopoulos and Lignos 2020) comprising specimens without doubler plates in the panel zone is also used to further validate the accuracy of the proposed panel zone stiffness and Eq. (18) for both V_p and $V_{6\gamma_y}$. Referring to Fig. 12a, the proposed panel zone stiffness matches the experimental data relatively well. The maximum error is up to 15% and for only two cases. Referring to Fig. 12b, while the AISC (2016b) panel zone model does not depict the influence of column flange thickness, t_{cf}, on V_p, the proposed model is sufficient regardless of the panel zone geometry. Referring to Fig. 12c, same trends hold true for $V_{6\gamma_y}$. Notably, for cross-sections with $t_{cf} > 40$mm, the proposed model is remarkably better than the current state of the seismic design practice.

Effect of doubler plates

The impact of utilizing doubler plates, and their influence on the proposed model sufficiency is examined by means of supplemental CFE simulations featuring shallow and stocky (W14x398) as well as deep (W24x131) column cross-sections with a one-sided thick doubler plate ($t_{dp} > 40$mm). Table 3 summarizes the virtual test matrix. It is comprised of panel zones in which the doubler plates are either welded with CJP or fillets to the respective column. The respective details are shown schematically in Figs. 13a and 13b. Note that the examined welded configurations are consistent with the current practice (AISC 2016c; AWS 2016). The shallow and stocky column (W14x398) does not necessitate the presence of continuity plates according to the AISC (2016a) provisions. The doubler plate thickness is determined by the fillet radii of the column cross-section to avoid welding in its k-area (Lee et al. 2005). Since for both cross sections the fillet radii, r, used for detailing equals to 33 mm, this leads to a doubler plate thickness of $t_{dp} = 35$mm (1-3/8" in). The respective fillet welds have a leg thickness of $t_w = 48$ mm by assuming that the filler metal classification strength, $F_{EXX} = 1.2F_{ycw}$ (F_{ycw}: yield stress of the column web base material). The calculated fillet weld material thickness satisfies the AISC (2016c) provisions. The doubler plate yield stress is assumed to be $F_{ydp} = 1.1F_{ycw}$. Neither plug welding nor horizontal welding on top and bottom of the doubler plates is necessary for the examined cases according to AISC (2016c). Either way, the above weld details would have increased the shear stress compatibility between the doubler plate and the column web. The column region is modelled with the same procedures discusser earlier. The doubler plate, which extends by $0.5d_b$ from the beam flanges, is modelled with quadratic brick elements with reduced integration (C3D20R). These are used to better capture the stress distribution through thickness of the doubler plate. Hard contact, that allows separation but not penetration, is employed between the doubler plate and the column web. In turn, the double plate is tied with the welding material, which was modeled explicitly as shown in Fig. 13.

Three loading histories are employed: a monotonic, a ramped cyclic symmetric (AISC 2016c) and a collapse-consistent loading protocol (Suzuki and Lignos 2020) to account for potential accumulation of doubler plate shear stress incompatibility throughout the loading history. The shear stress incompatibility between the doubler plate and the column web is quantified based the relative difference between the average shear stresses in the column web, $\bar{\tau}_{cw}$, and doubler plates, $\bar{\tau}_{dp}$; that is $(\bar{\tau}_{cw} - \bar{\tau}_{dp})/\bar{\tau}_{dp}$.

Figures 14a and 14b show the above metric with respect to the accumulated panel zone shear distortion, $\Sigma\gamma$, for deep (W24x131) as well as shallow and stocky (W14x398) columns, respectively. Prior to panel zone yielding (i.e., γ_y), the stresses in the column web are higher than those in the doubler plate by 10 to 30%, depending on the cross section and the weld specification. However, once both the doubler plate and the column web yield, the relative difference of their shear stress demand is not more than -10%. This is attributed to the fact that the yield stress of the doubler plate is purposely assumed to be 10% higher than that of the column web. This indicates no evident stress incompatibility between the doubler plate and the column web.

Referring to Figs. 14a and 14b, the use of a CJP weld provides higher shear stress compatibility (more than 90%) compared to fillet welded doubler plates (70-80% at shear distortions lower than γ_y). It is also observed that the relative difference is initially higher for stocky and shallow columns compared to deep ones. However, after panel zone yielding, this difference diminishes. This is more apparent in Fig. 14c under the collapse-consistent loading protocol regardless of the examined column cross-section. In brief, Fig. 14 suggests that the doubler plate ineffectiveness is not an issue for beam-to-column connections detailed according to AISC (2016c) and AWS (2016). For thick fillet-welded doubler plates, if the requirement for considerably thick fillet welds (so that the stresses impending from the column are properly attained by the doubler plate) is met, the doubler plate(s) and the column web attain fairly similar shear stresses. Therefore, the total panel zone thickness, including the double plate(s) (i.e., $t_{pz} = t_{cw} + t_{dp}$), may be directly employed in Eqs. (4), (17) and (18). Figure 15 illustrates indicative comparisons between the proposed model and data from full-scale beam-to-column joints with doubler plates retrieved from the analyzed inelastic panel zone cases.

The authors are of the opinion that the doubler plate-to-column web shear-stress incompatibility, which was mostly highlighted in prior studies on pre-Northridge beam-to-column connections

(Slutter 1981), is attributed to the uncertainty of the welding material and the weld specifications that were employed at that time. Differences in material properties between doubler plates (e.g., use of A36 plates) and the respective column (e.g., A992 or A572 Gr. 50) could have attributed to some of the reported differences.

Effect of axial load

This section examines how the axial load should be considered within the proposed model to design/model inelastic panel zones in end (exterior) and interior steel MRF beam-to-column connections. In the former, columns experience axial load variations due to the transient axial load component. Doubler plates are omitted in these simulations since this effect was separately examined in the previous section. Table 4 summarizes the virtual test matrix that was examined in this case. In brief, a gravity load ratio, P_g/P_y, of 15%, 30% and 50% is considered for interior columns, whereas $P_g/P_y = 15\%$ is assumed for end columns. The first two values are deemed reasonable based on nonlinear response history analyses of representative 4- and 8-story steel MRF designs (Elkady and Lignos 2014, 2015) according to current design specifications. The last gravity load ratio may be representative in existing high-rise steel MRF buildings designed prior to the 1994 Northridge earthquake (Bech et al. 2015). The axial load demand variation in end columns is depicted based on representative loading histories developed for experimental testing of steel MRF columns (Suzuki and Lignos 2020). In particular, the imposed axial load demand, P/P_y, varies from -10% (tension) to 40% (compression) for the 8-story and from 5% to 25% for the 4-story MRF as retrieved from Suzuki and Lignos (2020). This is coupled with the imposed same shear distortion demand as the interior columns.

According to the AISC (2016b) specifications, no reduction in the panel zone shear strength would be introduced if it was designed to attain inelastic deformations (i.e., $n < 0.75$). If the panel zone was designed to remain elastic [based on $R_{n,el.}$ from AISC (2016b) specifications], then a reduction based on the von Mises criterion (von Mises 1913) would be employed. In prior work by Kim et al. (2015), it was assumed that the axial load is only sustained by the column flanges. However, this does not hold true because the present study suggests that the column web contribution in sustaining the axial load demand may be up to 40%. As such, in the proposed model, n, accounts for the full column cross-section with regard to the axial yield strength calculation. The relative difference between the panel zone shear resistance with/without the applied axial load throughout the loading history is computed as $(V_{pz}^{n=0} - V_{pz}^{n>0})/V_{pz}^{n=0}$, to evaluate the influence of the axial load.

Interior columns

Figure 16 shows the relative difference of interest versus the accumulated panel zone shear distortion, $\sum\gamma$, for the examined interior columns. In the same figure, a line is superimposed representing the relative difference according to AIJ (2012). The two plots of this figure are not schematically comparable, since the panel zone shear distortion history differs in both cases. Moreover, due to the imposed cyclic loading history, the relative difference attains zero when the panel zone shear strength attains zero as well. It is observed that the von Mises criterion, which is adopted by AIJ (2012) and AISC (2016b) for elastic panel zone design, corresponds well with the results regardless of the $\sum\gamma$ level. However, for inelastic panel zone design that no reduction in strength would be applied according to AISC (2016b), the panel zone shear resistance is overestimated by more than 10% for $P_g/P_y > 30\%$, depending on the cross-section. However, the above gravity load ratio range is uncommon in contemporary steel MRF designs (Elkady and Lignos 2014, 2015; Suzuki and Lignos 2020).

End columns

Figure 17 depicts the reduction in shear strength for both interior and end column panel zones for an 8-story MRF. It is observed that applying the von Mises criterion only for the applied gravity load leads to marginally unconservative results (~10%). Therefore, the panel zone shear strength reduction should be applied for the absolute peak load ratio P/P_y including the transient axial load component. For a 4-story MRF, the panel zone shear strength reduction is negligible (less than 4%) due to the decreased axial load variation in end columns.

Limitations of the present study

The proposed panel zone model neglects the influence of the composite action on the panel zone behavior. This is an important aspect to be considered (Castro et al. 2005; El Jisr et al. 2019; Elkady and Lignos 2014; Kim and Engelhardt 2002). On the other hand, practical methods to decouple the slab from the steel column/panel zone are available (Chaudhari et al. 2019; Tremblay et al. 1997). While the effect of cyclic hardening on the panel zone shear strength was disregarded, during design basis earthquakes, capacity-designed steel MRFs are likely to experience modest lateral drift demands (i.e., 2%); therefore, the panel zone is likely to experience shear distortions of nearly $4\gamma_y$, depending on the panel zone-to-beam relative strength ratio. Cyclic hardening is fairly minor for this range of shear distortions; thus, the proposed model should predict fairly well the panel zone shear strength. Moreover, at seismic intensities associated with low probability of occurrence seismic events (i.e., 2% in 50 years) the steel MRF behavior is expected to be asymmetric due to ratcheting (Lignos et al. 2011, 2013). Shake table collapse experiments (Lignos et al. 2013; Suita et al. 2008) suggest that the panel zone inelastic behavior is fairly similar with that depicted by the examined collapse-consistent loading protocol. Moreover, The use of A36 doubler plates with A992 Gr. 50 steel columns was not investigated. While this practice appeared to be a default choice in pre-Northridge steel MRF designs, the use of A572 Gr. 50 doubler plates with A992 Gr. 50 steel columns appears to be the current practice in modern seismic-resistant steel MRFs. Finally, the proposed model should be further validated for beam-to-column connections comprising hollow structural columns.

Summary and Conclusions

This paper presents a new panel zone model for the seismic design and analysis of beam-to-column panel zone joints in capacity-designed moment-resisting frames (MRFs). The proposed model, which is developed on the basis of structural mechanics, reflects the realistic stress distributions within a panel zone joint geometry. These distributions are extracted from continuum finite element (CFE) models, which are thoroughly validated to available experimental data from pre- and post-Northridge interior and exterior subassemblies. We propose improved equations to predict the panel zone stiffness and shear strength at discrete levels of panel zone shear distortion pertinent to the balanced design of steel MRF beam-to-column joints according to current seismic provisions.

The CFE simulation results underscore that the commonly used assumption of uniform shear yielding is only valid in panel zone geometries featuring stocky and shallow column cross-sections regardless of the inelastic shear distortion level.

The elastic stiffness, K_e [see Eq. (4)], of the proposed panel zone model considers both shear and bending deformations based on shear strength equilibrium within the panel zone. Hence, its performance in predicting the elastic stiffness of slender panel zones (beam-to-column depth ratios, $d_b/d_c \geq 1.5$) is superior compared to available models in the literature as well as the ones available in current seismic provisions.

The proposed equation [see Eq. (17)] for the panel zone shear strength at yield, V_y (i.e., shear distortion of γ_y), matches that of the Krawinkler (1978) model for panel zones that are shear deformation-dominant (i.e., stocky cases) but performs much better in cases that the bending contribution is appreciable.

Comparisons with available full-scale test data suggest that the proposed model predicts the panel zone shear strength, V_p, [see Eq. (18) and Table 2] at a shear distortion of $4\gamma_y$ with a noteworthy accuracy even when panel zones feature columns with relatively thick flanges (i.e., $t_{cf} \geq 40$mm). The current model in the AISC (2016b) seismic specifications overpredicts V_p by 20% to 50% depending on the panel zone geometry. In that respect, the proposed model addresses a well-known limitation of available models in the literature.

The CFE simulations reveal that the commonly assumed value of $0.03K_e$ for the stiffness beyond $4\gamma_y$ shear distortions is not justifiable in most panel zone geometries. This is due to the increased column flange contribution to the panel zone strength at large inelastic shear distortions ($\gamma > 4\gamma_y$). For this reason, we propose an expression to predict the panel zone shear strength, $V_{6\gamma_y}$ [see Eq. (18) and Table 2], at a shear distortion of $6\gamma_y$.

Based on the examined cases, it is also found that the doubler plate to column web shear stress incompatibility does not appear to be an issue for beam-to-column connections, which are detailed according to current seismic provisions and detailing criteria (AISC 2016c; AWS 2016). Consequently, neither fillet nor CJP welded doubler plates should be treated differently either by reducing their strength or by intentionally accounting for one of the two doubler plates (i.e., CEN 2005). The authors are of the opinion that the doubler plate ineffectiveness reported in the literature is mostly attributed to weld specifications and construction practices prior to the 1994 Northridge earthquake.

Supplemental CFE simulations suggest that the von Mises criterion (von Mises 1913) may still be used to reduce the predicted panel zone shear strength for both interior and end columns in steel MRFs regardless of the employed lateral loading history. The shear strength reduction should always be based on the peak axial compressive load imposed to the respective column including the transient axial component due to dynamic overturning effects.

Dedication

This paper is dedicated to the memory of Professor Helmut Krawinkler, former professor at Stanford University, who was among the first to identify the importance of the panel zone on the seismic behavior of steel moment-resisting frames in the early 1970s. Our study builds upon his uppermost contribution and would have not been possible without it.

Data Availability

Some or all data, models, or code generated or used during the study are available in a repository or online in accordance with funder data retention policies. Some or all data, models, or code that support the findings of this study are available from the corresponding author upon reasonable request.

Acknowledgements

This study is based on work supported by a Nippon Steel Corporation collaborative grant as well as an EPFL internal grant for the first and second authors. The financial support is gratefully acknowledged. The authors would like to sincerely thank Prof. Dr. Bozidar Stojadinovic from ETH-Zürich, for providing test data for the development of the inelastic panel zone database. Any opinions, findings, and conclusions or recommendations expressed in this paper are those of the authors and do not necessarily reflect the views of sponsors.

References

ABAQUS. (2014). *ABAQUS analysis user's manual version 6.14-1*. Dassault Systems Simulia Corp., RI, USA.

AIJ. (2012). *Recommendations for design of connections in steel structures*. Architectural Institute of Japan, Tokyo (in Japanese).

AISC. (2016a). *Prequalified connections for special and intermediate steel moment frames for seismic applications, ANSI/AISC 358-16*. Chicago, IL: American Institute for Steel Construction.

AISC. (2016b). *Specification for structural steel buildings, ANSI/AISC 360-16*. Chicago, IL: American Institute for Steel Construction.

AISC. (2016c). *Seismic provisions for structural steel buildings, ANSI/AISC 341-16*. Chicago, IL: American Institute for Steel Construction.

AWS. (2016). *Structural welding code-seismic supplement, AWS D1.8/D1.8M:2016*. American Welding Society, Miami, FL.

Bech, D., Tremayne, B., and Houston, J. (2015). "Proposed changes to steel column evaluation criteria for existing buildings." *2nd ATC-SEI Conf Improv. Seism. Perform. Exist. Build. Struct.*, Earthquake Engineering Research Institute, San Francisco, 255–272. https://doi.org/10.1061/9780784479728.022.

Bertero, V., Krawinkler, H., and Popov, E. P. (1973). *Further studies on seismic behavior of steel beam-column subassemblages*. Earthquake Engineering Research Center, University of California, Berkeley, California.

Brandonisio, G., De Luca, A., and Mele, E. (2012). "Shear strength of panel zone in beam-to-column connections." *J. Constr. Steel Res.*, 71, 129–142. https://doi.org/10.1016/j.jcsr.2011.11.004.

de Castro e Sousa, A., and Lignos, D. G. (2017). *Residual stress measurements of European hot-rolled I-shaped steel profiles*. Technical Rep. No. 231302, EPFL, Lausanne.

de Castro e Sousa, A., Suzuki, Y., and Lignos, D. (2020). "Consistency in solving the inverse problem of the Voce-Chaboche constitutive model for plastic straining." *J. Eng. Mech.*, 146(9), 04020097. https://doi.org/10.1061/(ASCE)EM.1943-7889.0001839.

Castro, J. M., Elghazouli, A. Y., and Izzuddin, B. A. (2005). "Modelling of the panel zone in steel and composite moment frames." *Eng. Struct.*, 27(1), 129–144. https://doi.org/10.1016/j.engstruct.2004.09.008.

CEN. (2005). *EN 1993-1-8: Eurocode 3: Design of steel structures - Part 1-8: Design of joints*. European Committee for Standardization, Brussels, Belgium.

Charney, F. A., Iyer, H., and Spears, P. W. (2005). "Computation of major axis shear deformations in wide flange steel girders and columns." *J. Constr. Steel Res.*, 61(11), 1525–1558. https://doi.org/10.1016/j.jcsr.2005.04.002.

Chaudhari, T., MacRae, G., Bull, D., Clifton, C., and Hicks, S. (2019). "Experimental behaviour of steel beam-column subassemblies with different slab configurations." *J. Constr. Steel Res.*, 162. https://doi.org/10.1016/j.jcsr.2019.105699.

Chi, B., and Uang, C.-M. (2002). "Cyclic response and design recommendations of reduced beam section moment connections with deep columns." *J. Struct. Eng.*, 128(4), 464–473. https://doi.org/10.1061/(ASCE)0733-9445(2002)128:4(464).

Chi, W. M., Deirlein, G. G., and Ingraffea, A. (1997). *Finite element fracture mechanics investigation of welded beam-column connections*. SAC Joint Venture, Cornell University, Ithaca, New York.

Chung, K., Kishiki, S., Matsumoto, Y., and Yamada, S. (2006). "Experimental study on the hysteresis behavior of panel subjected to multi-axial cyclic loadings." *J. Struct. Constr. Eng.*, 602, 203-210 (in Japanese).

Chung, K., Yamada, S., and Yang, I. (2010). “Simplified uni-axial hysteretic damage model for panel zone of structural steel under earthquake loads.” *Int. J. Steel Struct.*, 10(3), 267–281. https://doi.org/10.1007/BF03215836.

Ciutina, A. L., and Dubina, D. (2003). “Influence of column web stiffening on the seismic behaviour of beam-to- column joints.” *Proc. Conf. Behav. Steel Struct. Seism. Areas*, Naples, Italy, 269–275.

CSA. (2019). *Design of steel structures*. CAN/CSA S16-19, Mississauga, Canada: CSA.

El Jisr, H., Elkady, A., and Lignos, D. G. (2019). “Composite steel beam database for seismic design and performance assessment of composite-steel moment-resisting frame systems.” *Bull. Earthq. Eng.*, 17(6), 3015–3039. https://doi.org/10.1007/s10518-019-00564-w.

Elkady, A., and Lignos, D. G. (2014). “Modeling of the composite action in fully restrained beam-to-column connections: implications in the seismic design and collapse capacity of steel special moment frames.” *Earthq. Eng. Struct. Dyn.*, 43(13), 1935–1954. https://doi.org/10.1002/eqe.2430.

Elkady, A., and Lignos, D. G. (2015). “Effect of gravity framing on the overstrength and collapse capacity of steel frame buildings with perimeter special moment frames.” *Earthq. Eng. Struct. Dyn.*, 44(8), 1289–1307. https://doi.org/10.1002/eqe.2519.

Elkady, A., and Lignos, D. G. (2018a). “Full-scale testing of deep wide-flange steel columns under multiaxis cyclic loading: loading sequence, boundary effects, and lateral stability bracing force demands.” *J. Struct. Eng.*, 144(2), 04017189. https://doi.org/10.1061/(ASCE)ST.1943-541X.0001937.

Elkady, A., and Lignos, D. G. (2018b). “Improved seismic design and nonlinear modeling recommendations for wide-flange steel columns.” *J. Struct. Eng.*, 144(9), 04018162. https://doi.org/10.1061/(ASCE)ST.1943-541X.0002166.

El-Tawil, S., Vidarsson, E., Mikesell, T., and Kunnath, S. K. (1999). “Inelastic behavior and design of steel panel zones.” *J. Struct. Eng.*, 125(2), 183–193. https://doi.org/10.1061/(ASCE)0733-9445(1999)125:2(183).

FEMA. (1997). *Connection test summaries*. Federal Emergency Management Agency, Washington, DC.

Fielding, D. J., and Huang, J. S. (1971). “Shear in steel beam-to-column connections.” *Weld. Res. Suppl.*, 50(7), 313–326.

Ghobarah, A., Korol, R. M., and Osman, A. (1992). “Cyclic behavior of extended end- plate joints.” *J. Struct. Eng.*, 118(5), 1333–1353. https://doi.org/10.1061/(ASCE)0733-9445(1992)118:5(1333).

Gupta, A., and Krawinkler, H. (2000). “Dynamic P-delta effects for flexible inelastic steel structures.” *J. Struct. Eng.*, 126(1), 145–154. https://doi.org/10.1061/(ASCE)0733-9445(2000)126:1(145).

Han, S. W., Kwon, G. U., and Moon, K. H. (2007). “Cyclic behaviour of post-Northridge WUF-B connections.” *J. Constr. Steel Res.*, 63(3), 365–374. https://doi.org/10.1016/j.jcsr.2006.05.003.

Hjelmstad, K. D., and Haikal, G. (2006). “Analysis of steel moment frames with deformable panel zones.” *Steel Struct.*, 6(2), 129–140.

Jin, J., and El-Tawil, S. (2005). “Evaluation of FEMA-350 seismic provisions for steel panel zones.” *J. Struct. Eng.*, 131(2), 250–258. https://doi.org/10.1061/(ASCE)0733-9445(2005)131:2(250).

Kato, B., Chen, W. F., and Nakao, M. (1988). "Effects of joint-panel shear deformation on frames." *J. Constr. Steel Res.*, 10, 269–320. https://doi.org/10.1016/0143-974X(88)90033-8.
Kim, D.-W., Blaney, C., and Uang, C.-M. (2015). "Panel zone deformation capacity as affected by weld fracture at column kinking location." *Eng. J.*, 53(1), 27–46.
Kim, K. D., and Engelhardt, M. D. (2002). "Monotonic and cyclic loading models for panel zones in steel moment frames." *J. Constr. Steel Res.*, North American Special Issue, 58(5–8), 605–635. https://doi.org/10.1016/S0143-974X(01)00079-7.
Kim, S.-Y., and Lee, C.-H. (2017). "Seismic retrofit of welded steel moment connections with highly composite floor slabs." *J. Constr. Steel Res.*, 139, 62–68. https://doi.org/10.1016/j.jcsr.2017.09.010.
Krawinkler, H. (1978). "Shear in beam-column joints in seismic design of steel frames." *Eng. J.*, 15(3), 82–91.
Krishnan, S., and Hall, J. F. (2006). "Modeling steel frame buildings in three dimensions. I: panel zone and plastic hinge beam elements." *J. Eng. Mech.*, 132(4), 345–358. https://doi.org/10.1061/(ASCE)0733-9399(2006)132:4(345).
Lee, D., Cotton, S. C., Hajjar, J. F., Dexter, R. J., and Ye, Y. (2005). "Cyclic behavior of steel moment-resisting connections reinforced by alternative column stiffener details II. panel zone behavior and doubler plate detailing." *Eng. J.*, 42(4), 215–238.
Léger, P., Paultre, P., and Nuggihalli, R. (1991). "Elastic analysis of frames considering panel zones deformations." *Comput. Struct.*, 39(6), 689–697. https://doi.org/10.1016/0045-7949(91)90212-5.
Lemaitre, J., and Chaboche, J. L. (1990). *Mechanics of solid materials*. Cambridge, UK: Cambridge University Press.
Li, X.-S., and Goto, Y. (1998). "A three-dimensional nonlinear seismic analysis of frames considering panel zone deformations." *J. Struct. Mech. Earthq. Eng. JSCE*, 1998(605), 1–13. https://doi.org/10.2208/jscej.1998.605_1.
Lignos, D. G., Hikino, T., Matsuoka, Y., and Nakashima, M. (2013). "Collapse assessment of steel moment frames based on E-Defense full-scale shake table collapse tests." *J. Struct. Eng.*, 139(1), 120–132. https://doi.org/10.1061/(ASCE)ST.1943-541X.0000608.
Lignos, D. G., Krawinkler, H., and Whittaker, A. S. (2011). "Prediction and validation of sidesway collapse of two scale models of a 4-story steel moment frame." *Earthq. Eng. Struct. Dyn.*, 40(7), 807–825. https://doi.org/10.1002/eqe.1061.
Lin, K. C., Tsai, K. C., Kong, S. L., and Hsieh, S. H. (2000). "Effects of panel zone deformations on cyclic performance of welded moment connections." *12th WCEE*, Auckland, New Zealand, Paper No. 1252.
Lu, L. W., Ricles, J. M., Mao, C., and Fisher, J. W. (2000). "Critical issues in achieving ductile behaviour of welded moment connections." *J. Constr. Steel Res.*, 55(1–3), 325–341. https://doi.org/10.1016/S0143-974X(99)00092-9.
Lui, E. M., and Chen, W.-F. (1986). "Frame analysis with panel zone deformation." *Int. J. Solids Struct.*, 22(12), 1599–1627. https://doi.org/10.1016/0020-7683(86)90065-X.
Mao, C., Ricles, J., Lu, L. W., and Fisher, J. (2001). "Effect of local details on ductility of welded moment connections." *J. Struct. Eng.*, 127(9), 1036–1044. https://doi.org/10.1061/(ASCE)0733-9445(2001)127:9(1036).
von Mises, R. (1913). "Mechanik der festen körper im plastisch-deformablen zustand." *Nachrichten Von Ges. Wiss. Zu Gött. Math.-Phys. Kl.*, 1, 582–592.

Mulas, M. G. (2004). "A structural model for panel zones in non linear seismic analysis of steel moment-resisting frames." *Eng. Struct.*, 26(3), 363–380. https://doi.org/10.1016/j.engstruct.2003.10.009.
Ozkula, G., Harris, J., and Uang, C.-M. (2017). "Observations from cyclic tests on deep, wide-flange beam-columns." *Eng. J.*, 54(1), 45–60.
PEER/ATC. (2010). *Modeling and acceptance criteria for seismic design and analysis of tall buildings*. Prepared for Pacific Earthquake Engineering Research Center (PEER) by Applied Technology Council (ATC): Redwood City, CA.
Popov, E. P., Blondet, M., Stepanov, L., and Stojadinović, B. (1996). *Full-scale beam-column connection tests-Experimental investigations of beam-column subassemblages*. Report No. SAC-96/01, Part 2, Applied Technology Council (ATC), 555 Twin Dolphin Dr. Redwood City, Calif.
Qi, L., Paquette, J., Eatherton, M., Leon, R., Bogdan, T., Popa, N., and Nunez, E. (2018). "Analysis of fracture behavior of large steel beam-column connections." *Proc. 12th Int. Conf. Adv. Steel-Concr. Compos. Struct. - ASCCS 2018*, Universitat Politècnica València. https://doi.org/10.4995/ASCCS2018.2018.7122.
Ricles, J. M., Mao, C., Lu, L.-W., and Fisher, J. W. (2000). *Development and evaluation of improved details for ductile welded unreinforced flange connections*. SAC Joint Venture, Lehigh University, Bethlehem.
Ricles, J. M., Zhang, X., Lu, L.-W., and Fisher, J. W. (2004). *Development of seismic guidlines for deep-column steel moment connections*. ATLSS Report, Lehigh University, Bethlehem.
Shin, S. (2017). "Experimental and analytical investigation of panel zone behavior in steel moment frames." PhD Thesis, University of Texas at Austin.
Shin, S., and Engelhardt, M. D. (2013). "Experimental study on panel zone behavior in steel moment resisting frames." *7th Int. Symp. Steel Struct.*, Jeju, Korea.
Shirsat, P. S., and Engelhardt, M. D. (2012). "Preliminary analysis of doubler plate attachment details for steel moment frames." *15th WCEE*, Lisboa, Portugal.
Skiadopoulos, A., and Lignos, D. G. (2020). "Development of inelastic panel zone database." *J. Struct. Eng.*, under review.
Slutter, R. G. (1981). *Tests of panel zone behavior in beam-column connections*. Lehigh University, Bethlehem.
Soliman, A. A., Ibrahim, O. A., and Ibrahim, A. M. (2018). "Effect of panel zone strength ratio on reduced beam section steel moment frame connections." *Alex. Eng. J.*, 57(4), 3523–3533. https://doi.org/10.1016/j.aej.2018.07.017.
Suita, K., Yamada, S., Tada, M., Kasai, K., Matsuoka, Y., and Shimada, Y. (2008). "Collapse experiment on 4-story steel moment frame: Part 2 detail of collapse behavior." *Proc. 14th World Conf. Earthq. Eng.*, Beijing, China, Vol. 1217.
Suzuki, Y., and Lignos, D. G. (2020). "Development of collapse-consistent loading protocols for experimental testing of steel columns." *Earthq. Eng. Struct. Dyn.*, 49(2), 114-131. https://doi.org/10.1002/eqe.3225.
Tremblay, R., Tchebotarev, N., and Filiatrault, A. (1997). "Seismic performance of RBS connections for steel moment resisting frames: influence of loading rate and floor slab." *Proc. STESSA 97*, Kyoto, Japan.
Tsai, K. C., and Popov, E. P. (1988). *Steel beam-column joints in seismic moment resisting frames*. EERC Report 88-19, University of California, Berkeley, CA.

Wang, SJ. (1988). “Seismic response of steel building frames with inelastic joint deformation.” PhD Thesis, Department of Civil Engineering, Lehigh University, Bethlehem, PA.

Young, B. (1972). “Residual stresses in hot-rolled members.” *Paris*, 1–30.

Table 1. Statistical parameters for the linear regression curves of the $a_{eff} - K_f/K_e$ relationships

Location	Web			Flange		
Distortion level	γ_y	$4\gamma_y$	$6\gamma_y$	γ_y	$4\gamma_y$	$6\gamma_y$
Mean	0.91	1.1	1.2	0.019	0.063	0.073
Standard deviation	0.032	0.016	0.015	0.011	0.051	0.058
R^2	0.95	0.94	0.96	0.95	0.98	0.97

Table 2. Normalized average shear stress values and expressions in the web and the flanges, based on the proposed model

<table>
<tr><th rowspan="2" colspan="2">Equation</th><th colspan="2">Web ($a_{w,eff}$)</th><th colspan="2">Flange ($a_{f,eff}$)</th></tr>
<tr><th>$4\gamma_y$ (V_p)</th><th>$6\gamma_y$ ($V_{6\gamma_y}$)</th><th>$4\gamma_y$ (V_p)</th><th>$6\gamma_y$ ($V_{6\gamma_y}$)</th></tr>
<tr><td colspan="2">General case</td><td rowspan="3">1.1</td><td rowspan="3">1.15</td><td>$0.93(K_f/K_e) + 0.015$</td><td>$1.05(K_f/K_e) + 0.02$</td></tr>
<tr><td rowspan="2">Simplified case</td><td>Slender panel zone</td><td>0.02</td><td>0.03</td></tr>
<tr><td>Stocky panel zone</td><td>0.1</td><td>0.1</td></tr>
</table>

Table 3. Virtual test matrix for the examination of doubler plate effectiveness

Column	Beam	Doubler plate thickness [mm]	Welding type	Loading protocol
W14x398	W36x150	35	CJP	Cyclic symmetric
			Fillet	Monotonic
				Cyclic symmetric
				Collapse-consistent
W24x131	W30x108		CJP	Cyclic symmetric
			Fillet	Monotonic
				Cyclic symmetric
				Collapse-consistent

Table 4. Virtual test matrix for the examination of the axial load effect

Column	Beam	Number of stories	Joint location	P_g/P_y
W14x398	W36x150	-	interior	15%
				30%
				50%
		4	end	15%
		8		
W24x131	W30x108	-	interior	15%
				30%
				50%
		4	end	15%

List of Figures

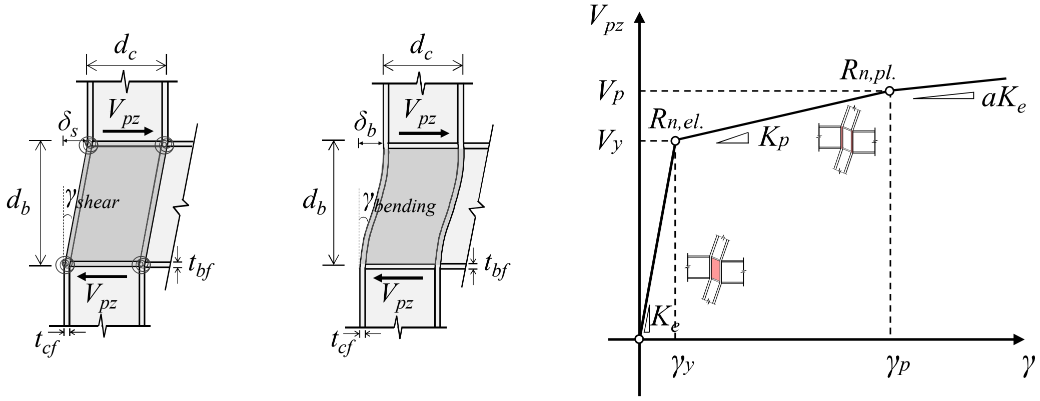

(a) Panel zone shear deformation (b) Panel zone bending deformation (c) Typical trilinear panel zone model

781 **Fig. 1.** Panel zone kinematics and mathematical model assumptions

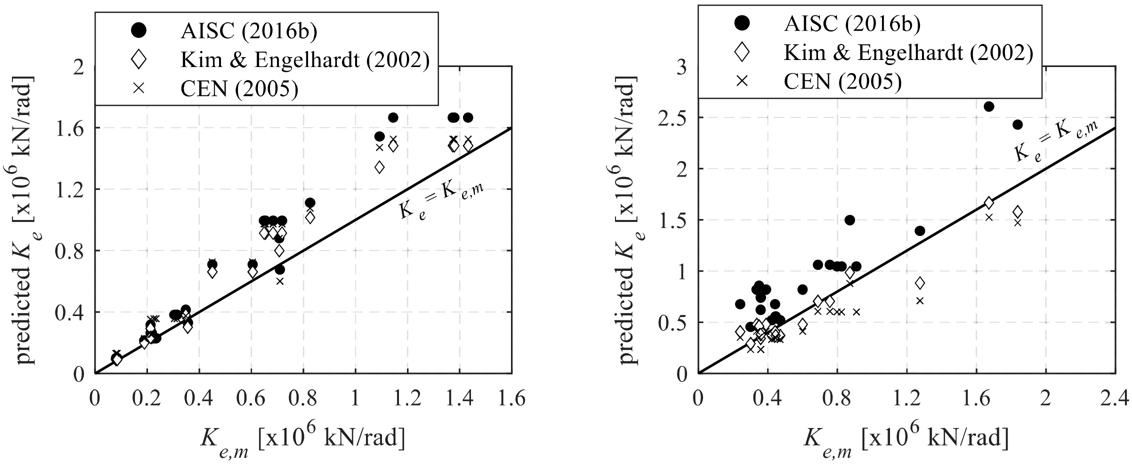

(a) test data without doubler plates (b) test data with doubler plates

Fig. 2. Comparison of analytically derived, K_e, and measured, $K_{e,m}$, panel zone elastic stiffness

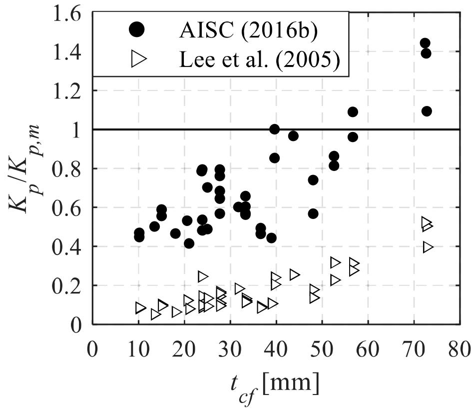

(a)

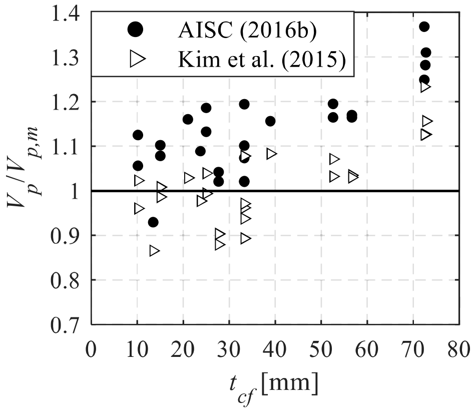

(b)

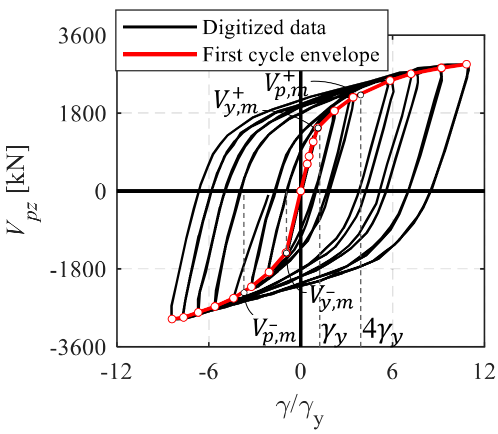

(c)

Fig. 3. Comparison of inelastic panel zone test data without doubler plate; (a) $K_p/K_{p,m}$ versus t_{cf} and (b) $V_p/V_{p,m}$ versus t_{cf} and (c) first cycle envelopes for panel zone measured shear stiffness and strength deduction (data extracted from Kim et al. (2015), specimen 3)

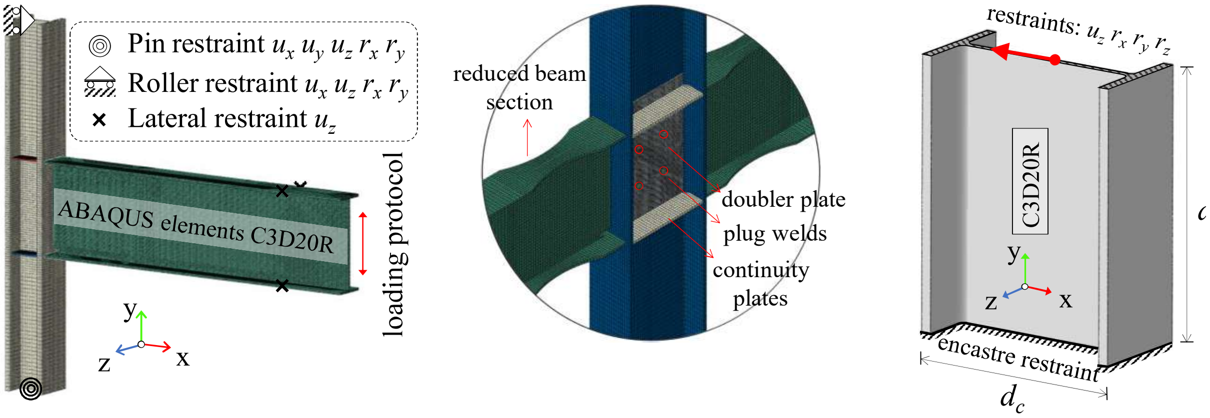

(a) detailed CFE model (b) doubler plate detailing (c) reduced-order CFE model

786 **Fig. 4.** Detailed and reduced-order continuum finite element models

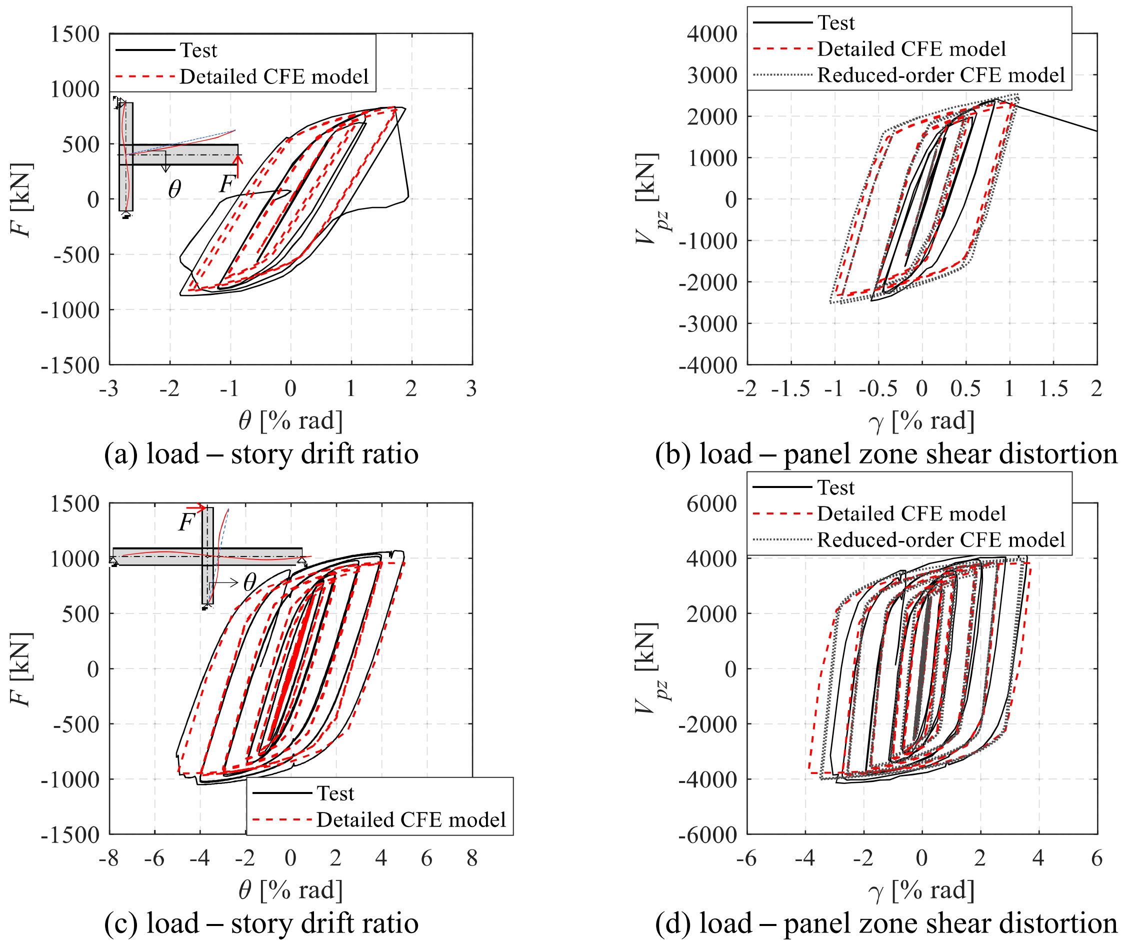

Fig. 5. Comparison between; CFE model prediction and test data; (a) and (b): data reproduced from FEMA (1997); (c) and (d): data reproduced from Ricles et al. (2004)

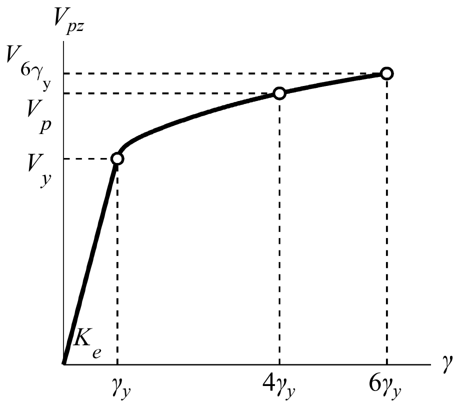

Fig. 6. Deduced panel zone performance parameters

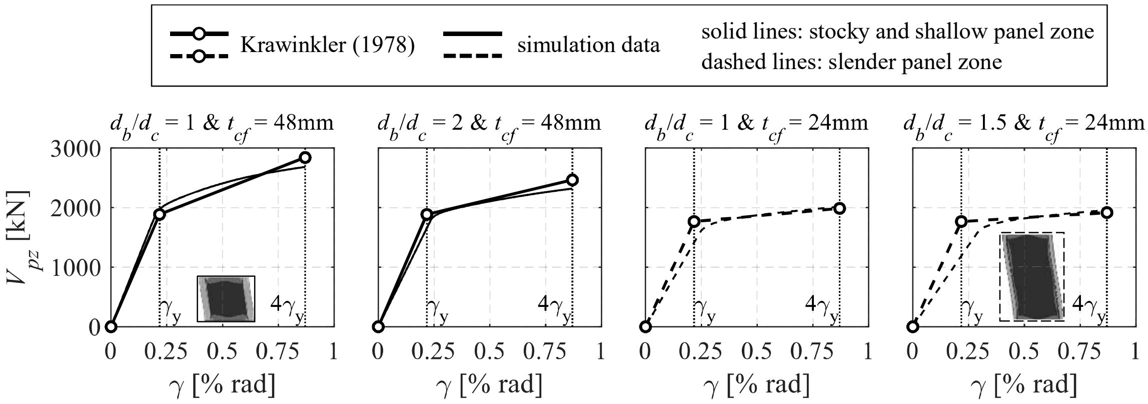

Fig. 7. Representative continuum finite element analysis results with varying web panel zone aspect ratio and column flange thickness

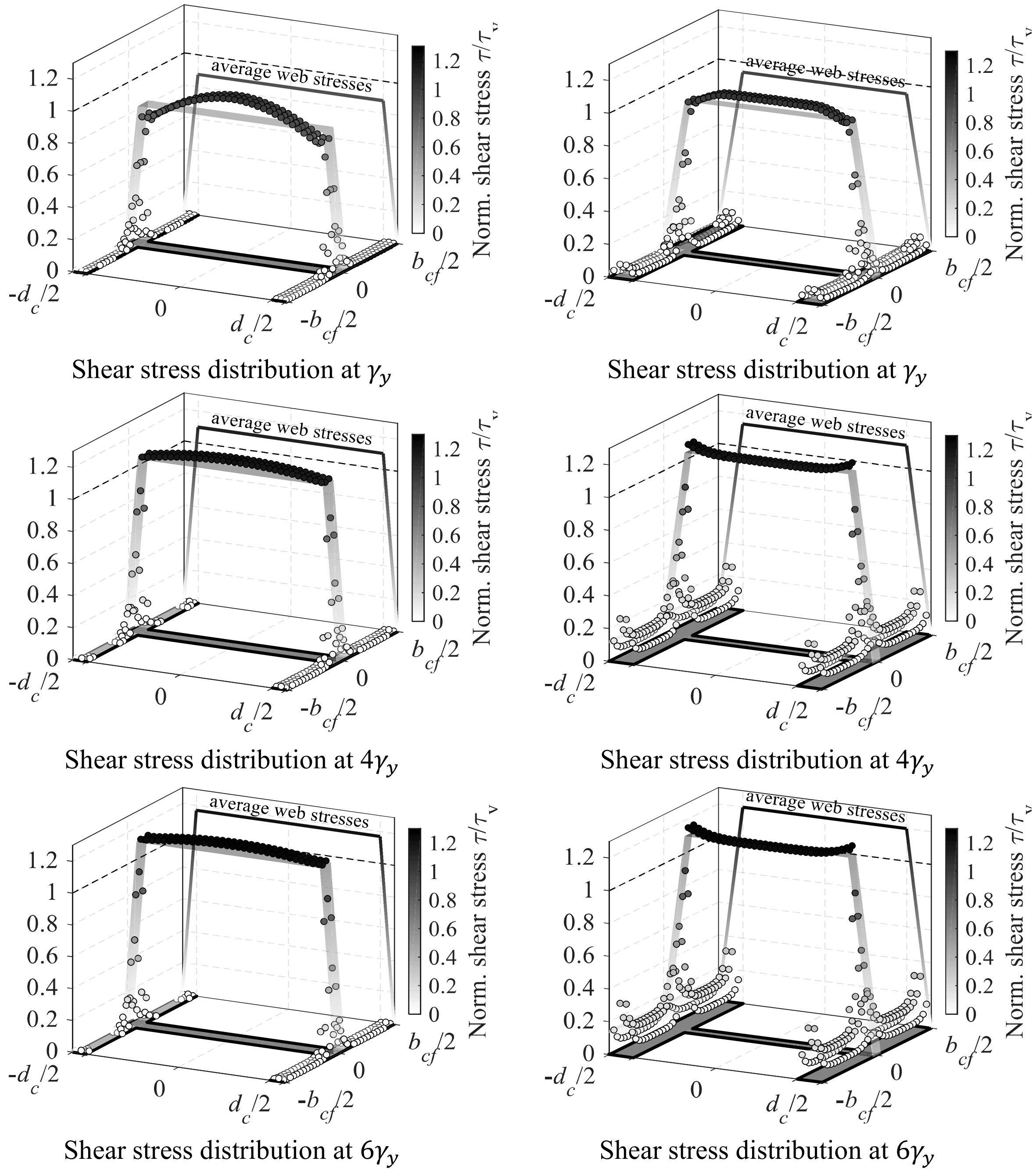

(a) slender panel zone (i.e., d_b/d_c = 1.5 and t_{cf} = 25mm)

(b) stocky and shallow panel zone (i.e., d_b/d_c = 1.0 and t_{cf} = 50mm)

Fig. 8. Shear stress distributions at γ_y, $4\gamma_y$ and $6\gamma_y$ for: (a) slender; (b) stocky and shallow panel zones

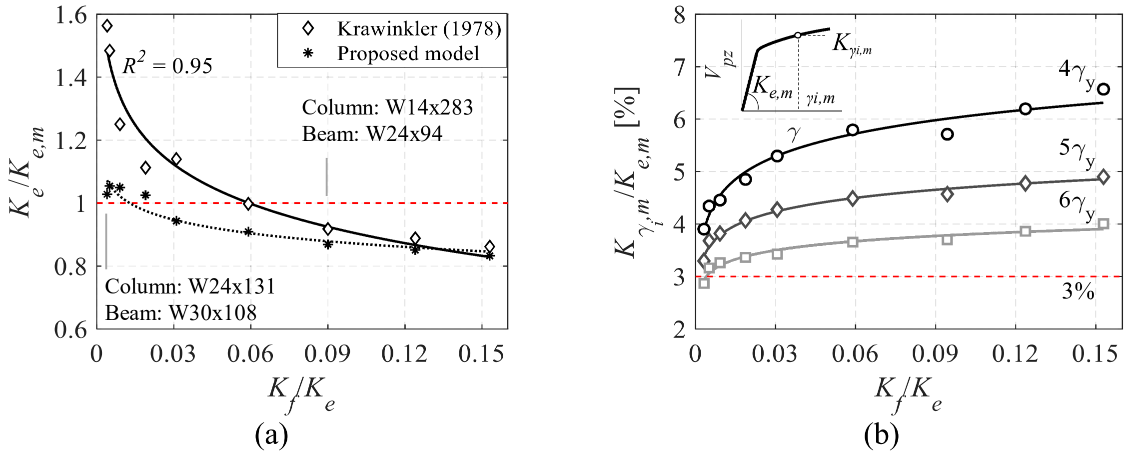

Fig. 9. (a) Deviation of predicted K_e from measured one, $K_{e,m}$, with respect to K_f/K_e and (b) normalized panel zone stiffness at representative shear distortion levels with respect to K_f/K_e

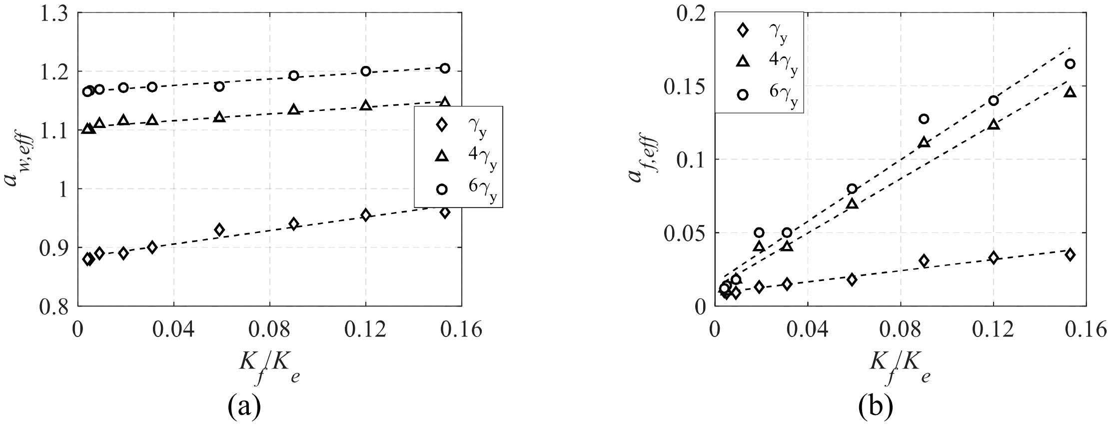

798 **Fig. 10.** Normalized average shear stress at γ_y, $4\gamma_y$ and $6\gamma_y$ for the (a) web and the (b) flange

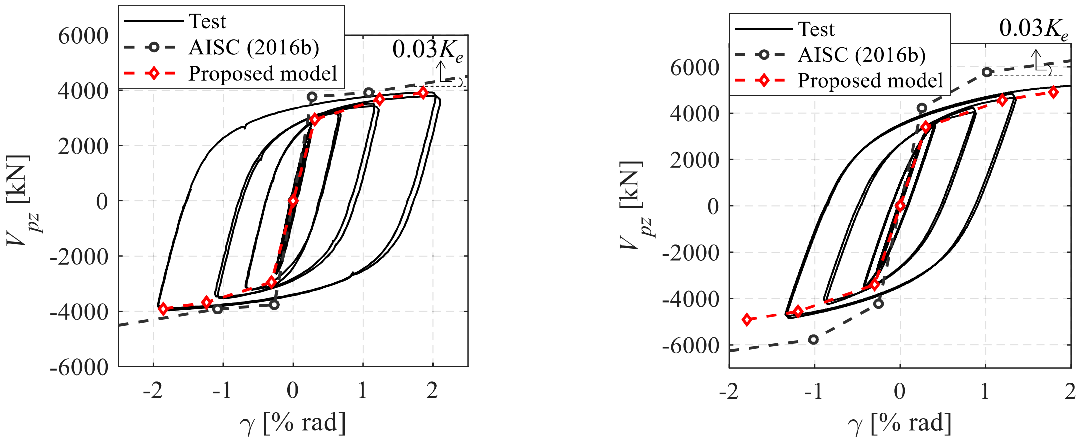

(a) Slender panel zone, $K_f/K_e = 0.003$ [Beam: W30x108, Column: W24x131, data reproduced from Ricles et al. (2004)]

(b) Stocky panel zone, $K_f/K_e = 0.07$ [Beam: W36x150, Column: W14x398, data reproduced from Shin (2017)]

Fig. 11. Comparison of measured and predicted panel zone hysteretic responses

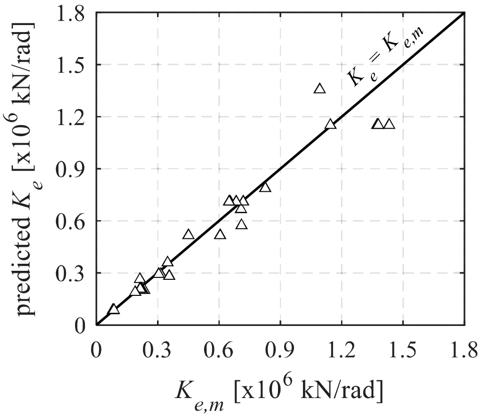

(a) $K_e/K_{e,m}$

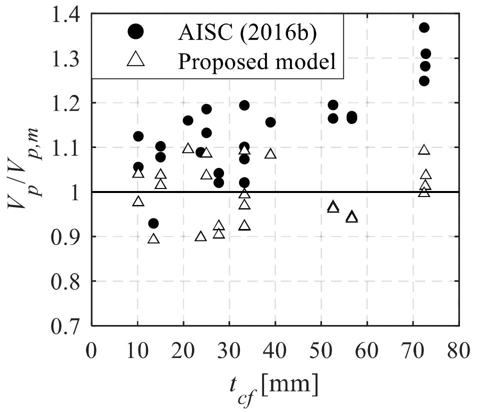

(b) $V_p/V_{p,m}$

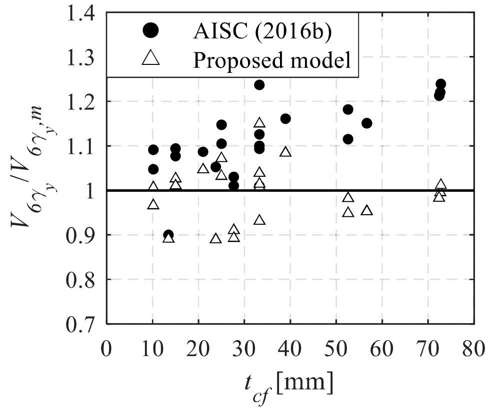

(c) $V_{6\gamma_y}/V_{6\gamma_{y,m}}$

Fig. 12. Comparison of the proposed panel zone stiffness and shear strength at $4\gamma_y$ and $6\gamma_y$ versus the measured ones from inelastic panel zone test data without doubler plates

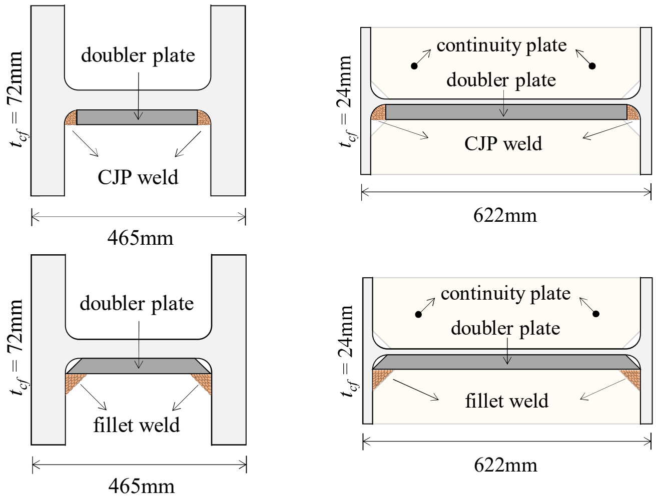

(a) Column: W14x398 (b) Column: W24x131

Fig. 13. Continuum finite element model CJP and fillet weld details

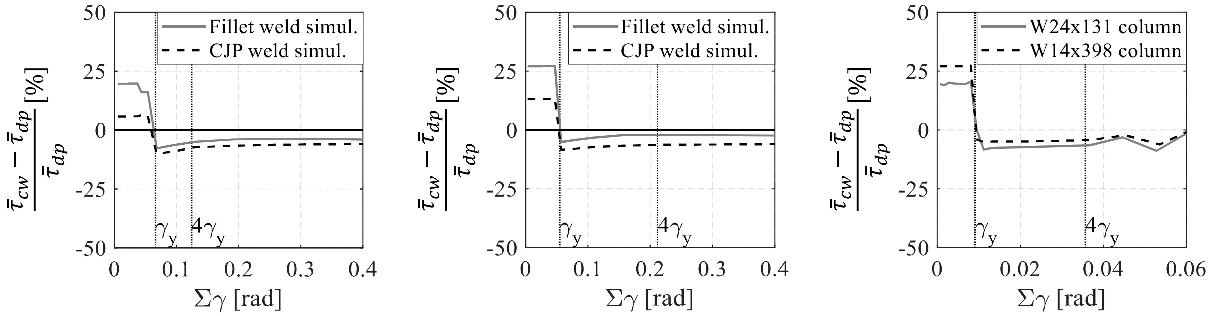

(a) Column: W24x131 – symmetric cyclic protocol

(b) Column: W14x398 – symmetric cyclic protocol

(c) collapse-consistent protocol

Fig. 14. Relative difference in the average shear stresses between the doubler plate and the column web versus accumulated panel zone shear distortion

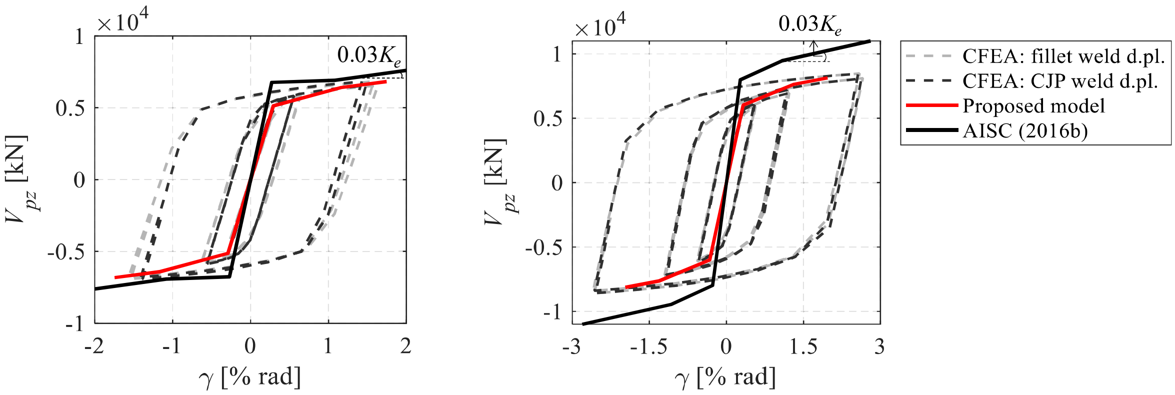

(a) W24x141 column (b) W14x398 column

Fig. 15. Comparison of measured and predicted response of panel zones with fillet- and CJP-welded doubler plates

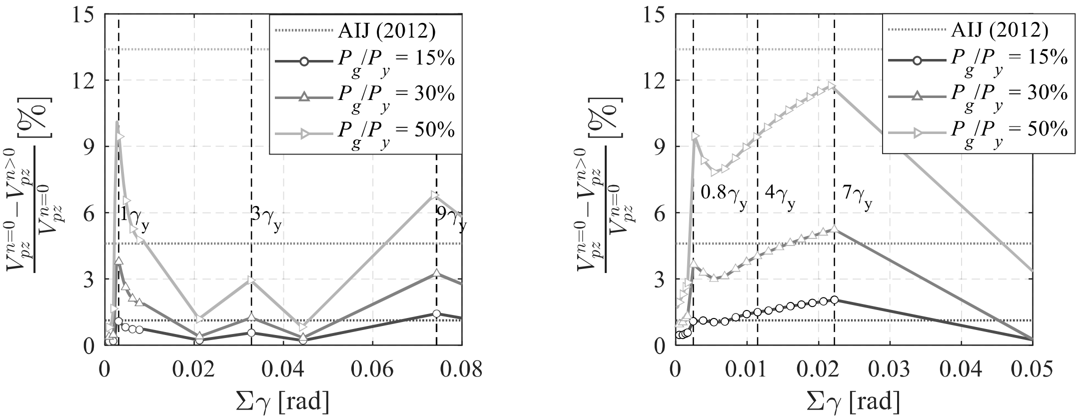

(a) W24x131 column (b) W14x398 column

Fig. 16. Panel zone relative difference between the panel zone shear strength with/without applied axial load versus accumulated panel zone shear distortion for interior columns

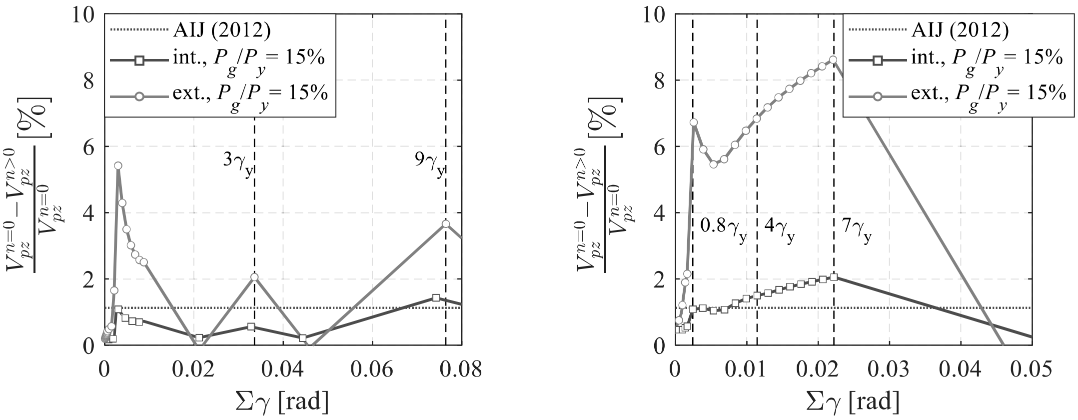

(a) W24x131 column (b) W14x398 column

Fig. 17. Panel zone relative reduction due to axial force versus accumulated panel zone shear distortion for both interior and exterior columns (8-story steel MRF)